2017 American Control Conference
Sheraton Seattle Hotel
May 24–26, 2017, Seattle, USA

Feedback-Linearization-based 3D Needle Steering in a Frenet-Serret Frame Using a Reduced Order Bicycle Model

Mohsen Khadem, Carlos Rossa, Nawaid Usmani, Ron S. Sloboda, Mahdi Tavakoli

***Abstract*— Robotics-assisted needle steering can enhance the performance of needle-based clinical procedures such as biopsy, brachytherapy, and drug delivery. We present an automated needle steering system capable of steering needles in 3D toward targets in tissue while avoiding anatomical obstacles. The system comprises a nonholonomic model of needle steering in tissue and a nonlinear controller for 3D trajectory tracking in soft tissue. First, a new reduced-order model of needle steering is presented. The proposed model is fully controllable and all the system states can be estimated on the fly. Next, the model is transformed to a local coordinate system using the Serret-Frenet formulation. By means of this transformation, the needle steering problem is converted to the regulation of the distance of the needle tip from a desired 3D trajectory. Finally, using the transformed model, a novel nonlinear controller is developed to steer the needle in 3D while avoiding anatomical obstacles. The control strategy is validated through simulations. The simulations indicate that the system is stable and can successfully follow a 3D trajectory. The results are promising, enabling future research in flexible needle path planning and control using the proposed reduced-order model and the controller.**

I. Introduction

Needle-based medical interventions are used for diagnostic and therapeutic applications such as biopsy, drug delivery, and cancer treatment. In needle insertions, long flexible needles with beveled tips are steered in soft tissue to reach designated targets. A needle with an asymmetric beveled tip has an uneven distribution of forces at the tip, which causes the needle to deflect from a straight path during the insertion. Using these needles, a surgeon can control the needle tip deflection by axially rotating the needle's base thus changing the orientation of the beveled tip. The term "*steering*" implies control of the needle tip deflection and controlling the direction of the needle tip trajectory as the needle is being inserted (see Fig. 1).

Robotics-assisted needle insertion can enhance the performance of needle-based surgeries. Modeling and control of continuum (continously flexible) robots with medical applications has been widely studied [1]–[7]. Park *et al.* developed a nonholonomic unicycle-like model to describe how an ideal needle with bevel tip moves through firm tissue [1]. They assumed that the needle tip motion in tissue is constrained to a circular path similar to a unicycle mobile robot. Webster *et al.* extended this idea and developed and experimentally validated kinematics-based model generalizing the unicycle model [2]. Several research groups have used classical beam theories to develop mechanics-based models of needle deflection [3].

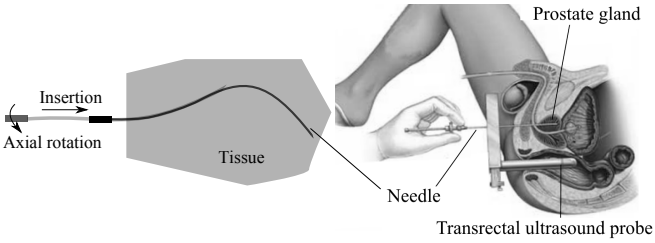

Fig. 1. A schematic of needle insertion in prostate brachytherapy. In brachytherapy a flexible needle is inserted in tissue, such that radioactive sources loaded in the needles can be placed in or near the tumor. The surgeon can steer the needle toward the target location by changing needle insertion velocity or axially rotating the beveled tip needle.

The nonholonomic unicycle model [2] is extensively used for needle steering. Kallem and Cowan presented the unicycle model in generalized coordinates and designed a linear observer to partially observe system states. The observations was used in a linear feedback control system for 2D needle steering [8]. Minhas *et al.* presented the idea of duty cycled spinning of the needle during insertion and showed that the curvature of the needle can be controlled via periodic needle rotations [9]. Rucker *et al.* proposed a sliding-mode controller based on the unicycle model and used it to track a desired trajectory within the tissue [10]. Waine *et al.* describe a method for controlling needle deflection in one plane through the use of an integrator backstepping control approach [11]. Patil *et al.* developed a needle steering strategy that relies on a rapid motion planner [12]. The planner incorporates the unicycle model to calculate the optimal needle axial rotations for steering the needle in 3D. Maghsoudi and Jahed introduced and simulated a model-based robust controller to address needle insertion in the presence of tissue parameter uncertainty [13]. We previously developed a nonlinear MPC controller for 2D needle steering using a mechanics-based model of needle insertion [14].

The 3D unicycle-like kinematic model [2] is nonlinear and most of its states cannot be directly measured during the needle insertion. Thus, most of the presented needle steering strategies can only steer the needle in 2D and

*This work was supported by the Natural Sciences and Engineering Research Council (NSERC) of Canada under grant CHRP 446520, the Canadian Institutes of Health Research (CIHR) under grant CPG 127768 and the Alberta Innovates - Health Solutions (AIHS) under grant CRIO 201201232.

M. Khadem, C. Rossa, and M. Tavakoli are with the Department of Electrical and Computer Engineering, University of Alberta, Edmonton, AB, T6G 2V4, Canada. {mohsen.khadem, rossa, mahdi.tavakoli}@ualberta.ca

R. S. Sloboda and N. Usmani are with the Cross Cancer Institute and the Department of Oncology, University of Alberta, Edmonton, AB, T6G 1Z2, Canada. {ron.sloboda, nawaid.usmani}@albertahealthservices.ca

neglect needle deflection out of the 2D plane [9], [13]–[15]. Researchers have attempted to use the unicycle model for 3D needle steering by developing nonlinear state observers for calculating unmeasurable system states [8], [16], [17], or by assuming that some of the model states are small and negligible [11]. Several 3D needle steering algorithms are developed by incorporating image-based algorithms for calculating the needle pose in 2D ultrasound images and consequently estimating unicycle model parameters [18].

In this paper, we present a new reduced-order nonholonomic model of needle steering. The proposed model is fully controllable and all of the system states can be estimated on the fly. Next, the proposed model is presented in a local coordinate system using the Serret-Frenet frame. By means of this transformation, the needle steering problem is converted to the regulation of the distance from a desired curved trajectory. Finally, using the transformed model, a novel nonlinear controller is developed to steer the needle in 3D while avoiding anatomical obstacles. The performance of the proposed approach is verified through several simulated scenarios.

This paper is organized as follows: Section II describes the 3D kinematic model of needle steering. Section III details the conversion of the system into the chained form and the control law that allows the path following. Details of the controller is presented in Section IV. Section V shows the validation results.

II. Reduced-order Model of Needle Steering

Here, we present a nonholonomic model of needle steering based on the bicycle model first presented in [2]. The bicycle model is a generalization of a nonholonomic mobile robot model and assumes that the needle is torsionally stiff and the insertions and twists applied to the needle base are directly transmitted to the tip. The motion of the needle is then fully determined by the motion of the needle tip. The needle tip bends under the asymmetric distribution of forces applied to the beveled tip and follows a path with a constant radius of curvautre in a plane defined by the orientation of the needle beveled tip. To track a desired 3D trajectory using the bicycle model, one needs to control the needle position and the needle tip orientation (6 states of the system). However, tracking the needle tip with a 2D imaging systems typically enable us to measure only the position of the needle and not its orientation (without the use of any observer). Here, we introduce a new reduce-order model of needle steering that can be simply implemented in needle steering.

Fig. 2 shows a schematic of 3D needle steering in tissue. An inertial coordinate frame $\{O\}$ is fixed on the needle point of entry and a local body-fixed frame $\{N\}$ is attached to the needle tip. The two frames initially coincide. Let $v, \omega \in \mathbb{R}$ denote the needle insertion velocity and the rotation speed expressed in the local frame. We use Z-Y-X rotation angles ϕ-ψ-θ around the local frame to parameterize the rotation of the needle tip. The beveled tip of the needle lies in the local $x'y'$ plane. Thus, the needle tip follows a constant curvature path in the $x'y'$ plane. The needle rotation along the y'-axis is assumed to be negligible, thus $\psi = 0$. Let the position of the origin of needle tip be $p = [x, y, z]^T$ in $\mathbb{R}^3$ relative to the inertial frame. Using this notation, the generalized coordinate of the needle tip is $q = [x, y, z, \phi, \theta]^T \in \mathcal{C}$, where $\mathcal{C} \subset \mathbb{R}^5$ is the configuration space (i.e., the space of all possible needle configurations).

The needle tip always follows a constant curvature path along the x' axis of the local frame at the velocity of v. It is also assumed that during the insertion, the needle tip rotation around z' axis is a linear function of the needle insertion velocity [2]:

$$\dot{\theta} = \kappa v \tag{1}$$

Here, κ is the needle tip deflection curvature and depends on the mechanical characteristics of the tissue and the needle. Considering two consecutive rotations around the local x' and y' axes, the rotation matrix ${}^{O}R_{N}$ allowing to rotate any vector from the local frame of the needle tip ($\{N\}$) to the inertial coordinate frame ($\{O\}$) is given by

$${}^{O}R_{N} = \begin{bmatrix} \mathrm{C}\theta & -\mathrm{S}\theta & 0 \\ \mathrm{C}\phi\mathrm{S}\theta & \mathrm{C}\phi\mathrm{C}\theta & -\mathrm{S}\phi \\ \mathrm{S}\phi\mathrm{S}\theta & \mathrm{S}\phi\mathrm{C}\theta & \mathrm{C}\phi \end{bmatrix} \tag{2}$$

Throughout this paper, shorthand notations S, C, T, and SC describe $\sin(\cdot)$, $\cos(\cdot)$, $\tan(\cdot)$, and $\sec(\cdot)$, respectively.

The needle tip (i.e., the steering wheel) always follows a constant curvature path along the x' axis of the local frame at the velocity of v. Thus, the needle tip velocity is zero in y' and z' directions in the needle tip local frame, i.e., ${}^{O}R_{N}^{T}\ [\dot{x} \quad \dot{y} \quad \dot{z}]^T = [v \quad 0 \quad 0]^T$. Using (2), we can construct the following constraints:

$$-\dot{x}\mathrm{S}\theta + \dot{y}\mathrm{C}\theta\mathrm{C}\phi + \dot{z}\mathrm{C}\theta\mathrm{S}\phi = 0 \tag{3a}$$

$$-\dot{y}\mathrm{S}\phi + \dot{z}\mathrm{C}\phi = 0 \tag{3b}$$

So far, we have three independent constraints given by (1), (3a), and (3b). (1) is a holonomic constraint and reduces the system's degrees of freedom (DoF) and the configuration space ($\mathcal{C}$) dimension to 4. (3a) and (3b) are nonholonomic constraints and decrease the DoF to 2. However, they do not introduce any loss of accessability in $\mathcal{C}$. We can write (3a) and (3b) as a set of Pfaffian constraints $A(q)\dot{q} = 0$, where

$$A = \begin{bmatrix} -\mathrm{S}\theta & \mathrm{C}\theta\mathrm{C}\phi & \mathrm{C}\theta\mathrm{S}\phi & 0 & 0 \\ 0 & -\mathrm{S}\phi & \mathrm{C}\phi & 0 & 0 \end{bmatrix} \tag{4}$$

Considering the 5-dimensional configuration space, the system of the 2 Pfaffian constraints in (4) and the single holonomic constraint in (1) entails that the admissible generalized velocities at each configuration q belongs to the 2-dimensional null space of matrix $A(q)$. Denoting by $\{g_1(q), g_2(q)\}$ a basis of the null space $\mathcal{N}(A(q))$, the admissible trajectories for the needle tip can be characterized as the solution of $g_1(q)u_1 + g_2(q)u_2$, where u_1 and $u_2 \in \mathbb{R}$ are the input vectors for the two remaining DoF. The bases of $\mathcal{N}(A(q))$ can be easily calculated from (4) as

$$\begin{aligned} g_1(q) &= [\mathrm{C}\theta \quad \mathrm{S}\theta\mathrm{C}\phi \quad \mathrm{S}\theta\mathrm{S}\phi \quad 0 \quad \kappa]^T \\ g_2(q) &= [0 \quad 0 \quad 0 \quad 1 \quad 0]^T \end{aligned} \tag{5}$$

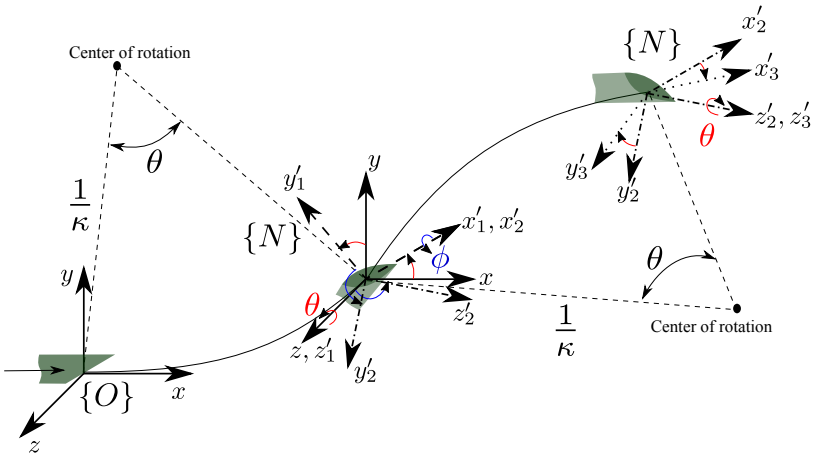

Fig. 2. A schematic of needle steering in tissue. An inertial coordinate frame O is fixed at the needle point of entry and the needle tip position is $[x, y, z]^T \in \mathbb{R}^3$. a local body-fixed frame N attached to the needle tip initially coincides with the inertial frame. The needle is inserted and follows a constant curvature path in $x'y'$ plane while rotating around the z'-axis with an angle of θ. The needle can also rotate axially by an angle ϕ. Needle rotation along the y'-axis is restricted by the surrounding tissue and is assumed to be negligible. The needle tip motion can be fully defined by a set of generalized coordinates $q = [x, y, z, \phi, \theta]^T$.

The bases are not unique, However. with the above selected bases the input vectors have a clear physical interpretation and are equal to the insertion velocity v and the rotation velocity ω. Now using (5) and (1), we can write the final kinematic model of needle steering as

$$\begin{bmatrix} \dot{x} \\ \dot{y} \\ \dot{z} \\ \dot{\phi} \\ \dot{\theta} \end{bmatrix} = \begin{bmatrix} \mathrm{C}\theta \\ \mathrm{S}\theta\mathrm{C}\phi \\ \mathrm{S}\theta\mathrm{S}\phi \\ 0 \\ \kappa \end{bmatrix} v + \begin{bmatrix} 0 \\ 0 \\ 0 \\ 1 \\ 0 \end{bmatrix} \omega \tag{6}$$

(6) gives the *reduced* order system. The system in (6) is driftless and affine in the inputs. Thus, we can verify the systems controllablity using the accessibility rank condition, i.e., the system is controllable if $\dim(\overline{\Delta}(q)) = \dim(\mathcal{C})$, where $\overline{\Delta}$ is the involutive closure of $\Delta = \mathrm{span}\{g_1(q), g_2(q)\}$. Using Successive Lie brackets to calculate $\overline{\Delta}(q)$, we obtain

$$\begin{aligned} &\dim(\overline{\Delta}) = \dim(\Delta_3) = \\ &\dim(\mathrm{span}\{g_1, g_2, [g_1, g_2], [g_1, [g_1, g_2]], [g_2, [g_1, g_2]]\}) \end{aligned} \tag{7}$$

(7) indicates that the system in (6) is controllable with a nonholonomy degree of 3. In the next sections, we will use the model to design a controller for 3D needle steering and guiding the needle to follow a desired path.

III. Transformation to Frenet-Serret Frame

Here, we transform the reduce-order model of needle steering, using a Frenet-Serret frame placed on an arbitrary desired 3D trajectory. By means of the transformation to the Frenet-Serret frame, the needle steering problem is converted to the regulation of the distance of the needle tip from a desired curved trajectory without the need for observing or direct control of the needle tip orientation. In differential geometry, the Frenet-Serret frame is commonly used to describe the kinematic properties of a particle moving along a continuous, differentiable curve in 3D. Following this approach, the needle tip motion is expressed in terms of the desired path parameters (curvilinear abscissa s, path curvature c, and path torsion τ).

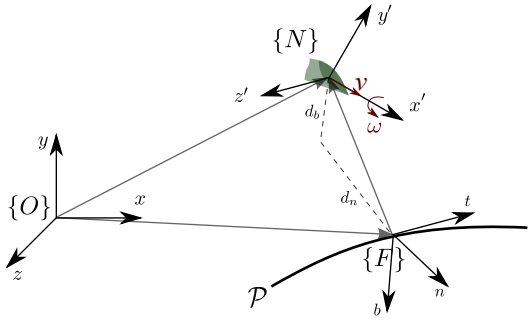

Fig. 3. Illustration of the needle path following problem.

The needle tip and the path ($\mathcal{P}$) to be followed are presented in Fig. 3, where $\{F\}$ is the orthogonal projection of the needle tip frame $\{N\}$ on the path. The tangent, normal, and bi-normal unit vectors of the Frenet-Serret frame associated with $\{F\}$ are t, n, and b. Let d_n and d_b denote the signed distances between frame $\{N\}$ and the origin of frame $\{F\}$. Let s be the path's abscissa, c the path's curvature, and τ its torsion. c and τ are assumed to be continuous bounded functions of s with bounded derivatives. Based on Frenet-Serret formulas, the angular velocity of F is given by ${}^F W_F = [\tau\dot{s} \;\; 0 \;\; c\dot{s}]^T$. The goal of the path following problem is to set the needle tip distance from the path (d_n and d_b) to zero, while aligning the linear velocity of the needle tip v with the tangent of the reference path t via manipulation of needle tip angular velocity ω. Let ${}^F R_N(\phi_e, \psi_e, \theta_e)$ be the rotation matrix from the Frenet-Serret frame to the needle frame, which aligns the velocity vector and tangent vector to the path t. ${}^F R_W$ is locally parameterized by Z-Y-X Eulerian angles. Writing the linear velocity of the needle frame in the

Frenet-Serret frame yields

$$ {}^{F}R_{N}(\phi_e,\psi_e,\theta_e){}^{N}V_N = {}^{F}V_F + \frac{d^{F}\overrightarrow{FN}}{dt} + {}^{F}W_F \times {}^{F}\overrightarrow{FN} \quad (8) $$

where ${}^{N}V_N = [v \;\; 0 \;\; 0]^T$ is the vector velocity of needle tip in needle frame $\{N\}$, ${}^{F}V_F = [\dot{s} \;\; 0 \;\; 0]^T$ is the $\{F\}$ frame linear velocity and, ${}^{F}\overrightarrow{FN} = [0 \;\; d_n \;\; d_b]^T$ is the vector of needle tip position in frame $\{F\}$.

We can also compute the needle frame angular velocity relative to the Frenet-Serret frame as

$$ {}^{N}W_{N,F} = {}^{N}W_N - {}^{N}R_F(\phi_e,\psi_e,\theta_e){}^{F}W_F \quad (9) $$

where ${}^{N}W_N = [0 \;\; 0 \;\; \kappa v]^T + R^T(\theta)[\omega \;\; 0 \;\; 0]^T$, and ${}^{N}W_{N,F}$ is given by

$$ {}^{N}W_{N,F} = \begin{bmatrix} \dot{\phi}_e \\ 0 \\ 0 \end{bmatrix} + R^T(\phi_e) \begin{bmatrix} 0 \\ \dot{\psi}_e \\ 0 \end{bmatrix} + \left(R(\psi_e)R(\phi_e)\right)^T \begin{bmatrix} 0 \\ 0 \\ \dot{\theta}_e \end{bmatrix} \quad (10) $$

Solving (8) for $\dot{s}$, $\dot{d_n}$ and $\dot{d_b}$ and (9) for $\dot{\phi_e}$, $\dot{\psi_e}$ and $\dot{\theta_e}$ gives the transformed system:

$$ \dot{s} = \frac{v\mathrm{C}\theta_e\mathrm{C}\psi_e}{1-d_nc} \quad (11a) $$

$$ \dot{d_n} = d_b\tau\dot{s} + v\mathrm{C}\psi_e\mathrm{S}\theta_e \quad (11b) $$

$$ \dot{d_b} = -d_n\tau\dot{s} - v\mathrm{S}\psi_e \quad (11c) $$

$$ \dot{\phi_e} = \omega\mathrm{C}\theta - \tau\dot{s}\mathrm{C}\theta_e\mathrm{SC}\psi_e + \kappa v\mathrm{C}\phi_e\mathrm{T}\psi_e + \omega\mathrm{S}\theta\mathrm{S}\phi_e\mathrm{T}\psi_e \quad (11d) $$

$$ \dot{\psi_e} = \omega\mathrm{S}\theta\mathrm{C}\phi_e + \tau\dot{s}\mathrm{S}\theta_e \quad (11e) $$

$$ \dot{\theta_e} = \kappa v\mathrm{C}\phi_e\mathrm{SC}\psi_e + \omega\mathrm{S}\theta\mathrm{S}\phi_e\mathrm{SC}\psi_e - \dot{s}\tau\mathrm{C}\theta_e\mathrm{T}\psi_e - c\dot{s} \quad (11f) $$

We note that in (11) $|d_n| < 1/c(s)$, which means that the transformation exists if the distance between the needle tip and the desired path $\mathcal{P}$ is not too large (smaller than the lower bound of the curve radii). Also, to avoid singularities in (3), $\psi_e, \theta_e \in (-\pi/2, \pi/2)$. Finally, we remark that the 3D Serret-Frenet frame transformation presented here is singular if the trajectory is a straight-line, since the normal direction of the straight-line could be either right or left direction. One way to avoid the singularity is using a path with a very small curvature rather than a completely straight line. Another way for avoiding the transformation singularity is using the parallel transport frame suggested in [19]. In the next section, we will use the model in (11) to design a controller to stabilize the needle distance from the path, i.e, d_n and d_b, at zero. Note that by means of the transformation to the Frenet-Serret frame, the needle steering problem is converted to the stabilization of the coordinates d_n and d_b.

IV. Regulation via Feedback Linearization

The objective of the needle steering controller is to synthesize a control law that allows the needle tip to follow a desired path in a stable manner, independent of the sign of the insertion velocity. We select the needle rotation velocity ω as the control input. Considering the needle insertion velocity v and its derivative are bounded, the needle steering problem consists of finding smooth feedback control laws $\omega(v, s, d_n, d_l, \phi_e, \psi_e, \theta_e)$ such that $\lim_{t\to\infty} d_n(t) = \lim_{t\to\infty} d_b(t) = 0$.

To design the controller, first the kinematic equations in (11) are transformed into the chain form via a change of state and control variables. The conversion of multi-input nonholonomic systems into the chained form was first presented by Bushnell *et al.* [20]. Let us determine a change of coordinates $(s, d_n, d_b, \phi_e, \theta_e, v, \omega) \to (z_1, z_2, z_3, u_1, u_2)$ allowing to transform (11) into the 3-dimensional chained system

$$ \begin{aligned} \dot{z}_1 &= u_1 \\ \dot{z}_2 &= u_1 z_3 \\ \dot{z}_3 &= u_2 \end{aligned} \quad (12) $$

First, we set $z_1 = s$. Thus u_1 is given by (11a). Then, the second state variable is chosen as $z_2 = 0.5(d_n^2 + d_b^2)$. Using (11b) and (11c) and eliminating $\dot{s}$ by (11b) we have

$$ \dot{z}_2 = u_1 z_3 = u_1(1 - d_nc)(d_n\mathrm{T}\theta_e - d_b\mathrm{T}\psi_e\mathrm{SC}\theta_e) \quad (13) $$

Taking derivative of $\dot{z}_3$ in (13) with respect to time and replacing $\dot{s}, \dot{d_n}, \dot{d_b}, \dot{\phi_e}, \dot{\psi_e}$ and $\dot{\theta_e}$ by their values in (11), the input u_2 is obtained as

$$ u_2 = a_{11}\omega + a_{12} \quad (14) $$

where a_{11}, a_{12}, are given in (15).

We note that for $|d_n| < 1/c(s)$ and any $\theta_e, \psi_e \in (-\pi/2, \pi/2)$, $(s, d_n, d_l, \phi_e, \psi_e, \theta_e) \to (z_1, z_2, z_3,)$ defines a mapping between $\mathbb{R}^4 \times (-\pi/2, \pi/2)^2$ and $\mathbb{R}^3$. Also, the control variable involves the derivative of path curvature (c'), whose value is thus needed.

The objective of the controller is to asymptotically bring $z_2 = 0.5(d_n^2 + d_b^2)$ to zero and also ensures that the constraint on the distance to the path (i.e., $|d_n| < 1/c(s)$ is satisfied

$$ a_{11} = -(1 - d_nc)\Big[\mathrm{SC}\theta_e\mathrm{S}\theta\mathrm{SC}\psi_e\big(\mathrm{S}\phi_e(-d_n\mathrm{SC}\theta_e + d_b\mathrm{T}\theta_e\mathrm{T}\psi_e) + d_b\mathrm{SC}\psi_e\mathrm{C}\phi_e\big)\big)\Big] \quad (15a) $$

$$ \begin{aligned} a_{12} = \frac{v\mathrm{C}\psi_e}{1-d_nc}\Big\{ & (d_n\mathrm{S}\theta_e\mathrm{C}\psi_e - d_b\mathrm{S}\psi_e)\,(d_nc' + cd_b\tau) + \\ & (cd_n - 1)\mathrm{C}\psi_e\Big(\mathrm{SC}\theta_e\left(-(cd_n-1)\mathrm{SC}^2\psi_e(d_b\kappa\mathrm{SC}\psi_e\mathrm{S}\phi_e + d_n\kappa\mathrm{SC}\theta_e\mathrm{C}\phi_e) + 1\right) - 1\Big) + \\ & \mathrm{T}\theta_e\left(d_b\mathrm{T}\psi_e\left(\kappa(cd_n-1)\mathrm{SC}\theta_e\mathrm{SC}^2\psi_e\mathrm{C}\phi_e + 2c\right) + (1-2cd_n)\mathrm{S}\theta_e\right)\Big)\Big\} \end{aligned} \quad (15b) $$

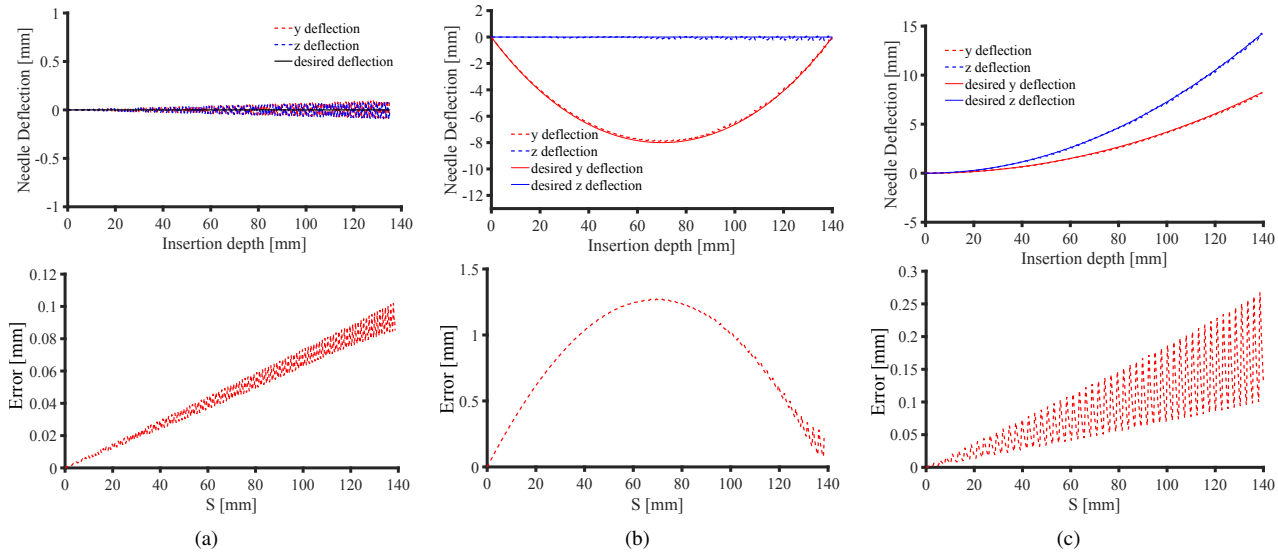

Fig. 4. Simulated results of needle steering for (a) needle insertion on a straight line, (b) 2D needle insertion with obstacle avoidance, (3) tracking a 3D path with a constant curvature. desired and actual needle deflection along y and z, and mean absolute error of tracking are shown in the figures.

along the trajectories of the controlled system. We consider the following control law:

$$u_2 = -u_1 k_1 z_2 - |u_1| k_2 z_3, \quad (k_2, k_3 > 0) \tag{16}$$

It is then immediate to verify that the origin of the closed-loop subsystem is asymptotically stable when $u_1 = \dot{s}$, i.e., the velocity along the path is constant.

So far, we have assumed that the insertion velocity v is either imposed or prespecified. Thus, we can use v in (11a) to ensure $\dot{s}$ is constant. Now, the steering angular velocity w can be computed from (16) as

$$\omega = a_{11}^{-1}(u_1 - a_{12}) \tag{17}$$

Based on (15a) and following our assumptions that $|d_n| < 1/c(s)$ and $\theta_e, \psi_e \in (-\pi/2, \pi/2)$, ω in (17) is well defined when $\theta \in (0, \pi/2)$. Based on (6) and considering the small curvature κ of needle in tissue, this assumption is satisfied when $\theta(0) > 0$. Thus, it suffices to select a nonzero initial condition for the needle initial pose θ. Also, ω asymptotically increases when $d_n(t) = d_b(t) = 0$. This motion, typically known as duty-cycling, mimics a drilling behavior and stabilizes the needle when the tracking error is zero. Duty-cycling can increase tissue trauma in real practice. We can limit the needle rotation velocity in the proximity of the desired path to avoid the drilling motion of the needle.

V. Simulation Results

In this section, several simulations are performed to validate the proposed needle steering strategy. We will use the feedback of needle global position (x, y, and z) to control the needle tip to follow a desired trajectory. During the needle insertion, these values can be calculated online using an imaging system. By knowing the position of the needle and the desired path parameters (s, τ and c), the steering angular velocity can be computed from (17).

Three clinical scenarios are simulated:

TABLE I

Simulation results. Units are in mm.

	1st scenario	2nd scenario	3rd scenario
e_y	0.1	0.18	0.11
e_z	0.076	0.108	0.095
$RMSE$	0.081	0.12	0.091

1) The needle is steered on a straight line to reach a target placed at a depth of 140 mm. This is the most common goal in needle-based interventions, where the needle should be inserted along a straight line and the needle is only rotated to compensate for deviations from the straight path.
2) A 10 mm circular obstacle is positioned at a depth of 70 mm between the needle entry point into the tissue and the target. The needle is steered to reach a target at the depth of 140 mm while avoiding the obstacle.
3) The needle is steered on a 3D arbitrary curve with a constant radius of curvature.

We note that 3D Serret-Frenet frame transform presented in Section III is singular if the trajectory is a straight-line. In order to avoid this singularity, we assumed that the desired path in the first scenario has a very small curvature (0.0001 mm). In the 2nd scenario, the desired needle deflection in the z direction is zero and is a circular path with a radius of 130 mm in the y direction. The needle desired trajectory in the 3rd scenario is a 3D curve with constant radius of curvature of 600 mm. In the simulations, the needle curvature (κ) is set equal to 0.002 mm, which is selected based on the experimentally obtained mean radius of curvature for a 18G flexible brachytherapy needle [21]. We introduce 10% error in the measured value of κ to simulate uncertainty. Also, the maximum allowable rotation velocity is 10 radiant per second . The results are shown in Fig. 4.

Simulation results are summarized in Table I. The maxi-

mum error in the y direction, e_y, the maximum error in the z direction, e_z, and the root mean squared error (RMSE) of tracking are reported. The maximum tracking error is in the y direction in the 2nd scenario and it is equal to 0.18 mm. This error is below the accepted margin of error in clinical needle insertions (~ 5 mm) [14]. The results show that the controller is accurate, stable, and has a satisfactory performance.

VI. Concluding Remarks

In this paper, a new reduced-order model of needle steering is proposed by modifing a bicycle-like model of needle steering. Next, the kinematic model of needle steering is expressed in a chained format using a transformation to the Frenet-Serret frame. Finally, a feedback control law is proposed to stabilize the chained system. The proposed method was validated and analyzed through several simulations. The results show that the controller is accurate and stable. Future efforts will focus on validating the controller by performing experiments with biological tissue in a realistic testing scenario. Also, the reduced-order model presented in Frenet-Serret frame can be used with several other controllers. Further work is required to make the control laws robust in the presence of parametric uncertainty including saturation in the actuation signal and reject constant perturbations such as soft tissue reaction forces. In the future, our efforts will focus on developing nonlinear controller implementing other control inputs such as insertion velocity for more robust needle steering.

References

[1] W. Park, J. S. Kim, Y. Zhou, and *et al.*, "Diffusion-based motion planning for a nonholonomic flexible needle model," in *Robotics and Automation, 2005. ICRA 2005. Proceedings of the 2005 IEEE International Conference on*, 18-22 April 2005, pp. 4600–4605.

[2] R. J. Webster, J. S. Kim, N. J. Cowan, G. S. Chirikjian, and A. M. Okamura, "Nonholonomic modeling of needle steering," *The International Journal of Robotics Research*, vol. 25, no. 5-6, pp. 509–525, 2006.

[3] M. Khadem, C. Rossa, N. Usmani, R. S. Sloboda, and M. Tavakoli, "A two-body rigid/flexible model of needle steering dynamics in soft tissue," *IEEE/ASME Transactions on Mechatronics*, vol. 21, no. 5, pp. 2352–2364, Oct 2016.

[4] S. Misra, K. Reed, B. Schafer, and *et al.*, "Mechanics of flexible needles robotically steered through soft tissue," *Int. J. Rob. Res.*, vol. 29, no. 13, pp. 1640–1660, 2010.

[5] F. Alambeigi, S. Sefati, R. J. Murphy, I. Iordachita, and M. Armand, "Design and characterization of a debriding tool in robot-assisted treatment of osteolysis," in *2016 IEEE International Conference on Robotics and Automation (ICRA)*, May 2016, pp. 5664–5669.

[6] F. Alambeigi, Y. Wang, R. J. Murphy, I. Iordachita, and M. Armand, "Toward robot-assisted hard osteolytic lesion treatment using a continuum manipulator," in *2016 38th Annual International Conference of the IEEE Engineering in Medicine and Biology Society (EMBC)*, 2016, pp. 5103–5106.

[7] F. Alambeigi, R. Seifabadi, and M. Armand, "A continuum manipulator with phase changing alloy," in *2016 IEEE International Conference on Robotics and Automation (ICRA)*, 2016, pp. 758–764.

[8] V. Kallem and N. J. Cowan, "Image guidance of flexible tip-steerable needles," *IEEE Transactions on Robotics*, vol. 25, no. 1, pp. 191–196, 2009.

[9] D. Minhas, J. Engh, M. Fenske, and C. Riviere, "Modeling of needle steering via duty-cycled spinning," in *29th Annual International Conference of the IEEE Engineering in Medicine and Biology Society (EMBS)*, Aug 2007, pp. 2756–2759.

[10] D. Rucker, J. Das, H. Gilbert, P. Swaney, and *et al.*, "Sliding mode control of steerable needles," *IEEE Transactions on Robotics*, vol. 29, no. 5, pp. 1289–1299, Oct 2013.

[11] M. Waine, C. Rossa, R. Khadem, and *et al.*, "An integrator-backstepping control approach for out-of-plane needle deflection minimization," in *IEEE International Conference on Advanced Intelligent Mechatronics (AIM), Banff, Canada*, 2016, pp. 1598–1603.

[12] S. Patil, J. Burgner, R. Webster, and R. Alterovitz, "Needle steering in 3D via rapid replanning," *IEEE Transactions on Robotics*, vol. 30, no. 4, pp. 853–864, Aug 2014.

[13] A. Maghsoudi and M. Jahed, "Needle dynamics modelling and control in prostate brachytherapy," *IET Control Theory Applications*, vol. 6, no. 11, pp. 1671–1681, 2012.

[14] M. Khadem, C. Rossa, R. Sloboda, and *et al.*, "Ultrasound-guided model predictive control of needle steering in biological tissue," *Journal of Medical Robotics Research*, vol. 01, no. 01, p. 1640007, 2016.

[15] C. Rossa, M. Khadem, R. Sloboda, and *et al.*, "Constrained optimal control of needle deflection for semi-manual steering,," in *IEEE International Conference on Advanced Intelligent Mechatronics (AIM), Banff, Canada*, 2016, pp. 1198–1203.

[16] B. Fallahi, C. Rossa, R. Sloboda, and *et al.*, "Partial estimation of needle tip orientation in generalized coordinates in ultrasound image-guided needle insertion," in *IEEE International Conference on Advanced Intelligent Mechatronics (AIM), Banff, Canada*, 2016, pp. 1604–1609.

[17] M. Motaharifar, H. A. Talebi, and *et al.*, "Adaptive observer-based controller design for a class of nonlinear systems with application to image guided control of steerable needles," in *American Control Conference (ACC)*, 2012, pp. 4849–4854.

[18] G. J. Vrooijink, M. Abayazid, S. Patil, and *et al.*, "Needle path planning and steering in a three-dimensional non-static environment using two-dimensional ultrasound images," *The International Journal of Robotics Research*, 2014.

[19] V. Cichella, I. Kaminer, V. Dobrokhodov, E. Xargay, R. Choe, N. Hovakimyan, A. P. Aguiar, and A. M. Pascoal, "Cooperative path following of multiple multirotors over time-varying networks," *IEEE Transactions on Automation Science and Engineering*, vol. 12, no. 3, pp. 945–957, July 2015.

[20] L. Bushnell, D. Tilbury, and S. Sastry, "Steering three-input nonholonomic systems: The fire truck example," *The International Journal of Robotics Research*, vol. 14, no. 4, pp. 366–381, 1995.

[21] M. Khadem, C. Rossa, R. Sloboda, and *et al.*, "Introducing notched flexible needles with increased deflection curvature in soft tissue," in *IEEE International Conference on Advanced Intelligent Mechatronics (AIM), Banff, Canada*, 2016, pp. 1186–1191.